Analysis, comparison and performance evaluation of wind turbine grid synchronizing methods

A. S. Mäkinen [#1], H. Tuusa [#1]

[#]*Department of Electrical Energy Engineering, Tampere University of Technology*
Korkeakoulunkatu 3, FI-33101, Tampere, Finland
[1] anssi.makinen@tut.fi

Abstract— **This paper studies the performance of wind turbine synchronizing methods SRF-PLL, DDSRF-PLL and DSOGI-FLL during three-phase and two-phase grid faults as well as under the presence of grid voltage harmonics. The goal of the study is to investigate how different methods can fulfil the primary task of the wind turbine which is to generate fundamental frequency positive sequence currents to the network. The contribution of the paper contains the comparison of the methods and the analysis of the impacts of tuning parameter selection on the operation of synchronizing methods. The study is carried out using Matlab/Simulink Simpower system using network model parameters taken from the real Finnish network.**

Keywords: Wind turbine, grid synchronization, SRF-PLL, DDSRF-PLL, DSOGI-FLL

I. INTRODUCTION

The main task of wind turbine (WT) is to generate electrical power by feeding currents to the network that contain only fundamental frequency positive sequence component in order to minimize grid disturbances and losses. This task is fulfilled if following two conditions are met: 1) the synchronous reference frame of vector controlled network side converter (NSC) is rotating with the angular frequency of fundamental frequency positive sequence component of the network voltage, 2) the current references for d- and q-axis components are constants. This study concentrates on the first requirement and the aim is to consider how different synchronizing methods can fulfil this task during network voltage disturbances.

In literature, comparisons of different synchronizing methods are also carried out. In [1] decoupled double synchronous reference frame – phase locked loop (DDSRF-PLL), dual second order generalized integrator – PLL (DSOGI-PLL) and enhanced three-phase PLL (3phEPLL) are compared under voltage sags, network voltage distortion and frequency deviation. However, the tuning parameters of the the different synchronizing methods are not expressed. In [2], the comparison between synchronous reference frame PLL (SRF-PLL), 3phEPLL, DSOGI-PLL, DDSRF-PLL and PLL found in PSCAD library are carried out. Again, the tuning parameters are not clearly expressed although it is informed that the settling time is 0.1s when the system is subjected to 1 Hz frequency sag. In [3], SRF-PLL, DDSRF-PLL and DSOGI-FLL are compared with a certain justified tuning parameters. This paper extends the work done in [3] and compares the performance of SRF-PLL, DDSRF-PLL and DSOGI-FLL during different network voltage disturbances with different tuning parameters. In addition to the comparison, the contribution of the paper is the analysis of how the selection of tuning parameters impact on the WT performance during different grid faults.

II. SRF-PLL

The block diagram of SRF-PLL system is illustrated in Fig. 1. The measured three-phase balanced grid voltages u_a, u_b, u_c are transformed into two axis αβ space vector components u_α and u_β using Clarke transformation [3][4]:

$$\underline{u}_{\alpha\beta} = \begin{bmatrix} u_\alpha \\ u_\beta \end{bmatrix} = [T_{\alpha\beta}] \begin{bmatrix} u_a \\ u_b \\ u_c \end{bmatrix} = \frac{2}{3} \begin{bmatrix} 1 & \frac{1}{2} & -\frac{1}{2} \\ 0 & \frac{\sqrt{3}}{2} & -\frac{\sqrt{3}}{2} \end{bmatrix} \begin{bmatrix} U\cos\theta \\ U\cos\left(\theta - \frac{2\pi}{3}\right) \\ U\cos\left(\theta - \frac{4\pi}{3}\right) \end{bmatrix} = U \begin{bmatrix} \cos\theta \\ \sin\theta \end{bmatrix} \quad (1)$$

where θ is the angular position of the grid voltage vector, U is the peak value of the phase voltage and $[T_{\alpha\beta}]$ is Clarke transformation matrix. After dq-transformation, the (1) can be expressed in rotating reference frame:

$$\underline{u}_{dq} = \begin{bmatrix} u_d \\ u_q \end{bmatrix} = \begin{bmatrix} \cos\theta_{sync} & \sin\theta_{sync} \\ -\sin\theta_{sync} & \cos\theta_{sync} \end{bmatrix} \begin{bmatrix} u_\alpha \\ u_\beta \end{bmatrix} = U \begin{bmatrix} \cos\theta_{sync}\cos\theta + \sin\theta_{sync}\sin\theta \\ -\sin\theta_{sync}\cos\theta + \cos\theta_{sync}\sin\theta \end{bmatrix} = U \begin{bmatrix} \cos(\theta - \theta_{sync}) \\ \sin(\theta - \theta_{sync}) \end{bmatrix} \quad (2)$$

where the angle θ_{sync} is the angular position of the rotating reference frame generated by the SRF-PLL. The PI-controller controls the q-component of the grid voltage to zero and its output is the angular frequency ω_{sync} of the PLL system. The feed forward term ω_{ff} is used to set the frequency near the final value in order to accelerate start-up process. The angular position θ_{sync} of the rotating reference frame is attained after integration of ω_{sync}. [3]

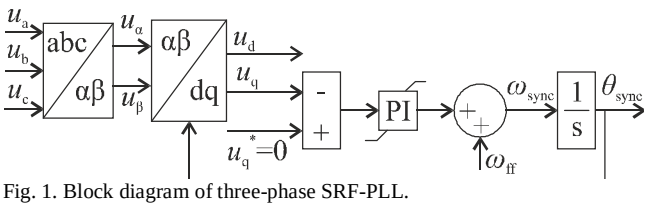

Fig. 1. Block diagram of three-phase SRF-PLL.

The voltage component of interest in (2) is the u_q since the purpose of the control system is to regulate the voltage q-component to zero. Due to the sinusoidal function in (2) the

system under consideration is nonlinear. However, when the phase difference θ-θ_{sync} is small the sinusoidal term behaves almost linearly. [5] The control system block diagram of Fig. 1 is redrawn after linearization of SRF-PLL as shown in Fig. 2 where k_{LF} and T_i represents the loop filter gain and integration time respectively.

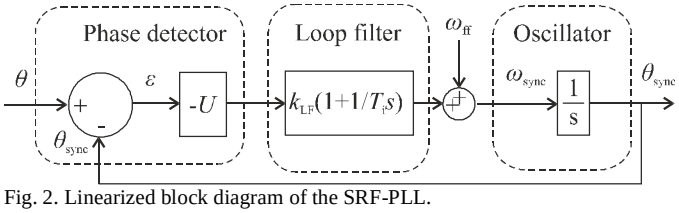

Fig. 2. Linearized block diagram of the SRF-PLL.

From the Fig. 2, it is possible to determine closed loop and closed loop error transfer functions. The transfer functions are utilized when the control parameters of the loop filter is determined. The closed-loop transfer function $H_{cl}(s)$ and the closed-loop error transfer function $H_{cl\varepsilon}(s)$ are: [6]

$$H_{cl}(s)=\frac{\theta_{sync}}{\theta}=\frac{PD(s)LF(s)VCO(s)}{1+PD(s)LF(s)VCO(s)}=\frac{k_{PLL}s+\frac{k_{PLL}}{T_i}}{s^2+k_{PLL}s+\frac{k_{PLL}}{T_i}} \quad (3)$$

$$H_{cl\varepsilon}(s)=\frac{\varepsilon(s)}{\theta}=1-H_{cl}(s)=\frac{s^2}{s^2+k_{PLL}s+\frac{k_{PLL}}{T_i}} \quad (4)$$

where k_{PLL} =-U*k_{LF}. The second order transfer functions (3) and (4) can also be expressed in normalized form with help of damping factor ζ and undamped natural frequency ω_n [6]

$$H_{cl}(s)=\frac{2\zeta\omega_n s+\omega_n^2}{s^2+2\zeta\omega_n s+\omega_n^2} \quad (5)$$

$$H_{cl\varepsilon}(s)=\frac{s^2}{s^2+2\zeta\omega_n s+\omega_n^2} \quad (6)$$

Combining (3) and (5), the undamped natural frequency ω_n and damping factor ζ can be expressed as a function of PLL gain k_{PLL} and integration time T_i and vice versa: [6]

$$\omega_n=\sqrt{\frac{k_{PLL}}{T_i}}\Rightarrow k_{PLL}=2\zeta\omega_n \quad (7)$$

$$\zeta=\frac{\sqrt{k_{PLL}T_i}}{2}\Rightarrow T_i=\frac{2\zeta}{\omega_n} \quad (8)$$

The second order transfer function (8) can also be expressed in following from: [9]

$$H_{cl}(s)=\frac{\frac{\omega_n^2}{\omega_z}(s+\omega_z)}{s^2+2\zeta\omega_n s+\omega_n^2}=\frac{\omega_n^2}{s^2+2\zeta\omega_n s+\omega_n^2}+\frac{\frac{\omega_n^2}{\omega_z}s}{s^2+2\zeta\omega_n s+\omega_n^2}=H_2(s)+\frac{s}{\omega_z}H_2(s) \quad (9)$$

where ω_z represents the root angular frequency of the nominator which is called zero frequency

$$2\zeta\omega_n s+\omega_n^2=0\Rightarrow s=-\frac{\omega_n^2}{2\zeta\omega_n s}=-\frac{\omega_n}{2\zeta s}=-\omega_z\,. \quad (10)$$

A. *Analysis of Second Order Transfer Function $H_2(s)$*

Left-hand side part of the $H_{cl}(s)$ in (9) corresponds to the basic 2nd order transfer function $H_2(s)$ and the right-hand side part contains the impact of zero to the system. The effect of parameters ω_n and ζ on the poles, which are the roots of the denominator, of the left-hand side part of (9) is depicted in Fig. 3. The undamped natural frequency ω_n corresponds to the distance between origo and transfer function poles and it is actual frequency in situation where the damping factor is zero. As the ζ increases, the angle φ rises and the absolute value of the real part of the pole σ increases. It should be noted that if the σ is negative the system is stable. The real part of the pole can be calculated with help of Fig. 3. [5]

$$\zeta=\sin\varphi=\frac{\sigma}{\omega_n}\Rightarrow\sigma=\omega_n\zeta \quad (11)$$

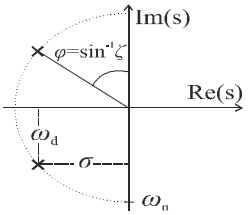

Fig. 3. Effect of parameters ω_n and ζ on the poles of $H_2(s)$.

Time constant of the response τ is defined as an inverse value of the σ. Thus, the time constant τ decreases as the σ increases. If the increase in value σ is made by increasing damping ζ the damped natural frequency ω_d decreases which increases the rise time of the response. On the other hand, the oscillations in step response decrease as the damping factor increase. The effect of ζ value to the step response of the system $H_2(s)$ is illustrated in Fig. 4a where the undamped natural frequency is set to 1. The settling time in Fig. 4a is defined in this case as the time measured from the start time to the time in which the system will stay within 2 % of the steady state value.

In Fig. 4b the effect of ω_n to the step response is analysed with a constant damping factor of 0.707. This damping factor produces phase angle φ of 45 degrees in Fig. 3, which seems to be optimum trade-off between rise time and overshoot. It can be seen from the Fig. 4b that the response is faster when ω_n is larger. The ω_n has no influence to the overshoot of the response which is solely determined by the damping factor.

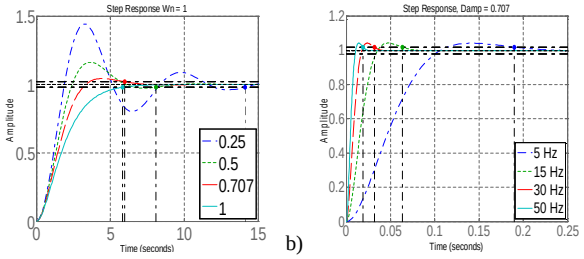

a) b)

Fig. 4. Step response of $H_2(s)$: a) constant ω_n, b) constant ζ.

B. *Analysis of Second Order Transfer Function $H_{cl}(s)$*

The step responses of the $H_{cl}(s)$ with different ζ are shown in Fig. 5a. The step response of the PLL transfer function

becomes more rapid, i.e. smaller settling and rise time, than ordinary 2nd order transfer function $H_2(s)$ with increased overshoot due to the action of zero. The increase in ζ decreases the value of ω_z as indicated by (10). This means that the zero moves toward origin and the impact of ω_z to the $s/\omega_z * H_2(s)$ becomes more important. The step responses of the $H_{cl}(s)$ with different ω_n are shown in Fig. 5b. The overshoot in $H_{cl}(s)$ is larger compared to overshoot in $H_2(s)$ shown in Fig. 5b due to the appearance of zero. The settling time decrease more as the value ω_n decrease due to the greater impact of zero. The zero moves further off the origin as the ω_n increases as indicated by (10). Thus, the effect of zero to the system operation decreases. However, the overshoot is independent of the value of the ω_n. The overshoot depends only on the damping factor as stated above.

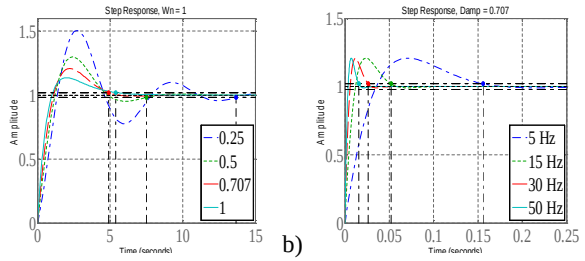

a) b)

Fig. 5. Step response of $H_{cl}(s)$: a) constant ω_n, b) constant ζ.

III. DDSRF-PLL

The DDSRF-PLL consists of a decoupling network and SRF-PLL. The decoupling network provides positive and negative sequence components from the input voltage vector. The synchronization to the positive sequence component of the grid voltage is achieved using SRF-PLL.

A. Decoupling Network

The unbalanced grid voltage vector $\underline{u}_{\alpha\beta}$ can be expressed in stationary reference frame as follows: [3]

$$\underline{u}_{\alpha\beta} = \begin{bmatrix} u_\alpha \\ u_\beta \end{bmatrix} = U^+ \begin{bmatrix} \cos(\omega t + \varphi^+) \\ \sin(\omega t + \varphi^+) \end{bmatrix} + U^- \begin{bmatrix} \cos(-\omega t + \varphi^-) \\ \sin(-\omega t + \varphi^-) \end{bmatrix} \quad (12)$$

where φ is initial angle and superscripts + and - correspond to the positive and negative sequence references. It is assumed that the positive sequence reference frame is rotating synchronously with the fundamental frequency positive sequence grid voltage component ($\theta_{sync}=\theta$). Thus, the positive and the negative sequence components can be expressed in synchronous dq-reference frame using angle θ_{sync} which is the output of the SRF-PLL. [5]

$$\underline{u}_{dq}^+ = \begin{bmatrix} u_d^+ \\ u_q^+ \end{bmatrix} = \begin{bmatrix} T_{dq}^+ \end{bmatrix} \begin{bmatrix} u_\alpha \\ u_\beta \end{bmatrix} = \begin{bmatrix} \cos(\theta_{sync}) & \sin(\theta_{sync}) \\ -\sin(\theta_{sync}) & \cos(\theta_{sync}) \end{bmatrix} \begin{bmatrix} u_\alpha \\ u_\beta \end{bmatrix} =$$
$$U^+ \begin{bmatrix} \cos(\varphi^+) \\ \sin(\varphi^+) \end{bmatrix} + U^- \cos(\varphi^-) \begin{bmatrix} \cos(2\omega t) \\ -\sin(2\omega t) \end{bmatrix} + U^- \sin(\varphi^-) \begin{bmatrix} \sin(2\omega t) \\ \cos(2\omega t) \end{bmatrix} \quad (13)$$

$$\underline{u}_{dq}^- = \begin{bmatrix} u_d^- \\ u_q^- \end{bmatrix} = \begin{bmatrix} T_{dq}^- \end{bmatrix} \begin{bmatrix} u_\alpha \\ u_\beta \end{bmatrix} =$$
$$U^- \begin{bmatrix} \cos(\varphi^-) \\ \sin(\varphi^-) \end{bmatrix} + U^+ \cos(\varphi^+) \begin{bmatrix} \cos(2\omega t) \\ \sin(2\omega t) \end{bmatrix} + U^+ \sin(\varphi^+) \begin{bmatrix} -\sin(2\omega t) \\ \cos(2\omega t) \end{bmatrix} \quad (14)$$

The left side terms in Equations (13) and (14) are DC-values and right side terms are AC-values. The DC-values are solved in order to distinguish the positive and the negative sequence components from the grid voltage:

$$U^+ \begin{bmatrix} \cos(\varphi^+) \\ \sin(\varphi^+) \end{bmatrix} = \begin{bmatrix} U_d^+ \\ U_q^+ \end{bmatrix} =$$
$$\begin{bmatrix} u_d^+ \\ u_q^+ \end{bmatrix} - U^- \cos(\varphi^-) \begin{bmatrix} \cos(2\omega t) \\ -\sin(2\omega t) \end{bmatrix} - U^- \sin(\varphi^-) \begin{bmatrix} \sin(2\omega t) \\ \cos(2\omega t) \end{bmatrix} \quad (15)$$

$$U^- \begin{bmatrix} \cos(\varphi^-) \\ \sin(\varphi^-) \end{bmatrix} = \begin{bmatrix} U_d^- \\ U_q^- \end{bmatrix} =$$
$$\begin{bmatrix} u_d^- \\ u_q^- \end{bmatrix} - U^+ \cos(\varphi^+) \begin{bmatrix} \cos(2\omega t) \\ \sin(2\omega t) \end{bmatrix} - U^+ \sin(\varphi^+) \begin{bmatrix} -\sin(2\omega t) \\ \cos(2\omega t) \end{bmatrix} \quad (16)$$

The decoupling network based on (15) and (16) and shown in Fig. 6 is used to cancel AC components from positive and negative sequence reference frames. The block LPF represents a simple first order low-pass filter with cut-off frequency of ω_f: [3]

$$LPF(s) = \frac{\omega_f}{s + \omega_f} \quad (17)$$

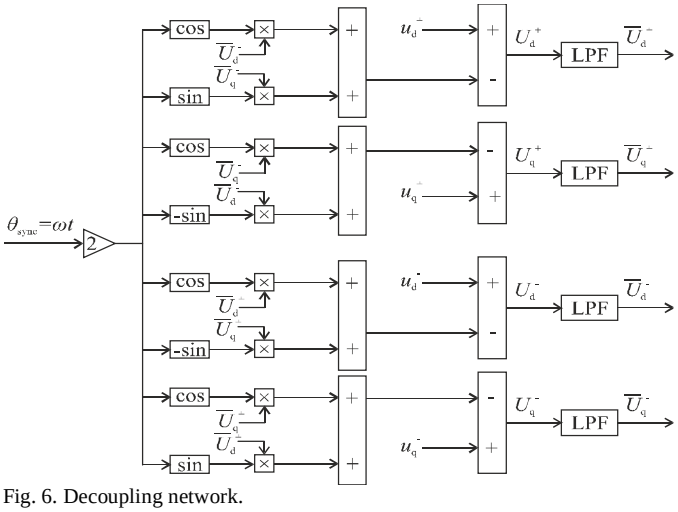

Fig. 6. Decoupling network.

The synchronization to the positive sequence component of the grid voltage is achieved when the positive sequence q-axis voltage component U_q^+ is zero. In that case, the initial phase angle φ^+ is zero and the positive sequence voltage component is aligned to d^+-axis rotating with angular speed of ω. The angle of positive sequence voltage component θ_{sync} is obtained using SRF-PLL. The block diagram of the DDSRF-PLL is shown in Fig. 7.

As can be seen from Fig. 2 the SRF-PLL system gain depends on the loop filter parameters as well as input voltage magnitude. If the input voltage drops, also the phase detector gain falls down. Thus, the controlled value U_q^+ is actively normalized to the amplitude of the positive sequence component of the grid voltage vector when DDSRF-PLL is used as shown in Fig. 7. [3][6]

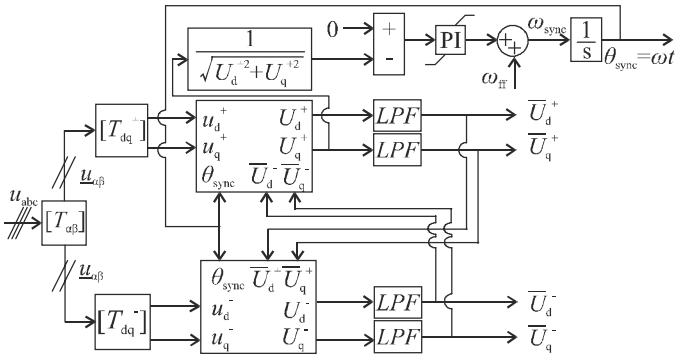

Fig. 7. The block diagram of DDSRF-PLL.

IV. DSOGI-FLL

DSOGI-FLL synchronization method utilizes the theory of instantaneous symmetrical components in order to extract the positive and negative sequence components from the grid voltage. The purpose of the DSOGI is to produce inquadrature axis components from the grid voltage vector components which are needed in positive and negative sequence calculation. The DSOGI is a bandpass filter which resonance frequency is actively tuned to the grid frequency. The tuning process is performed by the FLL.

A. Instantaneous grid voltage symmetrical components

The instantaneous positive and negative sequence components of network voltages can be calculated with help of $\alpha=e^{j2\pi/3}=e^{j120°}=-1/2+j*sqrt(3)/2$ which is called Fortesque operator. [3]

$$\begin{bmatrix} u_a^+ \\ u_b^+ \\ u_c^+ \end{bmatrix} = \frac{1}{3}\begin{bmatrix} 1 & \alpha & \alpha^2 \\ \alpha^2 & 1 & \alpha \\ \alpha & \alpha^2 & 1 \end{bmatrix}\begin{bmatrix} u_a \\ u_b \\ u_c \end{bmatrix} = [T_+]\begin{bmatrix} u_a \\ u_b \\ u_c \end{bmatrix} \tag{18}$$

$$\begin{bmatrix} u_a^- \\ u_b^- \\ u_c^- \end{bmatrix} = \frac{1}{3}\begin{bmatrix} 1 & \alpha^2 & \alpha \\ \alpha & 1 & \alpha^2 \\ \alpha^2 & \alpha & 1 \end{bmatrix}\begin{bmatrix} u_a \\ u_b \\ u_c \end{bmatrix} = [T_-]\begin{bmatrix} u_a \\ u_b \\ u_c \end{bmatrix} \tag{19}$$

The Equation (18) is transformed in to stationary reference frame using Clarke transformation (1).

$$\begin{bmatrix} u_\alpha^+ \\ u_\beta^+ \end{bmatrix} = [T_{\alpha\beta}]\begin{bmatrix} u_a^+ \\ u_b^+ \\ u_c^+ \end{bmatrix} = [T_{\alpha\beta}][T_+]\begin{bmatrix} u_a \\ u_b \\ u_c \end{bmatrix} = [T_{\alpha\beta}][T_+][T_{\alpha\beta}]^{-1}\begin{bmatrix} u_\alpha \\ u_\beta \end{bmatrix} = \tag{20}$$

$$\frac{1}{2}\begin{bmatrix} 1 & j \\ -j & 1 \end{bmatrix}\begin{bmatrix} u_\alpha \\ u_\beta \end{bmatrix} = \frac{1}{2}\begin{bmatrix} 1 & -q \\ q & 1 \end{bmatrix}\begin{bmatrix} u_\alpha \\ u_\beta \end{bmatrix} = [T_{\alpha\beta}^+]\begin{bmatrix} u_\alpha \\ u_\beta \end{bmatrix}$$

where the operator q is 90° phase shift operator i.e.

$$q = e^{-\frac{j\pi}{2}} \tag{21}$$

The negative sequence components from the αβ-grid voltage components can be calculated using (19)

$$\begin{bmatrix} u_\alpha^- \\ u_\beta^- \end{bmatrix} = [T_{\alpha\beta}][T_-][T_{\alpha\beta}]^{-1}\begin{bmatrix} u_\alpha \\ u_\beta \end{bmatrix} = \frac{1}{2}\begin{bmatrix} 1 & q \\ -q & 1 \end{bmatrix}\begin{bmatrix} u_\alpha \\ u_\beta \end{bmatrix} = [T_{\alpha\beta}^-]\begin{bmatrix} u_\alpha \\ u_\beta \end{bmatrix} \tag{22}$$

The positive and the negative sequence components can be identified from the grid voltage vector using matrixes $[T_{\alpha\beta}^+]$ and $[T_{\alpha\beta}^-]$ according to (20) and (22). However, in order to extract the positive and the negative sequence components from the grid voltage vector the 90° phase shift operator q is needed. The implementation of q is done using DSOGI.

B. DSOGI

DSOGI consists of two SOGIs which are second order adaptive band pass filters. One SOGI generates in line and 90° phase shifted components from input voltage component u_α in resonance frequency ω' and the other generates the same components from u_β. The structure of SOGI is shown in Fig. 8.

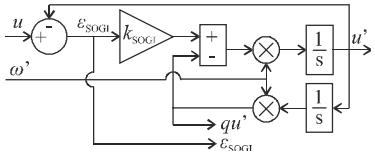

Fig. 8. Structure of DSOGI.

In Fig. 8 the u is the input voltage, u' is the output voltage in phase with the input voltage, qu' is the output voltage component in quadrature-phase with the input voltage, k_{SOGI} is the gain of the system, ε_{SOGI} is the error measure and ω' is the resonance frequency of the band pass filter. The transfer functions of the SOGI can be defined from Fig. 8: [3]

$$D(s) = \frac{u'}{u}(s) = \frac{k_{SOGI}\omega' s}{s^2 + k_{SOGI}\omega' s + \omega'^2} \tag{23}$$

$$Q(s) = \frac{qu'}{u}(s) = \frac{k_{SOGI}\omega'^2}{s^2 + k_{SOGI}\omega' s + \omega'^2} \tag{24}$$

$$E(s) = \frac{\varepsilon_{SOGI}}{u}(s) = \frac{s^2 + \omega'^2}{s^2 + k_{SOGI}\omega' s + \omega'^2} \tag{25}$$

The Bode plots of the transfer functions of $D(s)$ and $Q(s)$ with different values of gain k_{SOGI} are shown in Figs. 9a and 9b, respectively. The resonance frequency ω' was set to 2π*50Hz.

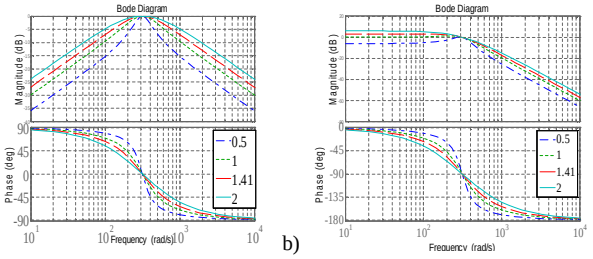

a) b)
Fig. 9. Bode plot: a) $D(s)$, b) $Q(s)$.

The bandwidth of the transfer functions are determined by the gain value k_{SOGI}. The higher the gain value the higher the bandwidth. Thus, the speed of the response increases as the gain increases. However, as the gain value k_{SOGI} decreases the selectivity of the filter increases. This implicates good harmonic rejection. It can be noticed from Equations (23)-(25) that the poles of the second order transfer functions are placed to have damping factor ζ=0.707 when the gain is set to k_{SOGI} = 1.41(sqrt2).

The purpose of the SOGI is to produce in line and 90° phase shifted components from input voltage component in resonance frequency ω'. These components are utilized as building blocks of the matrix $[T_{\alpha\beta}^+]$ and $[T_{\alpha\beta}^-]$ in (20) and (22) as follows:

$$\begin{bmatrix} u_\alpha^+ \\ u_\beta^+ \end{bmatrix} = \begin{bmatrix} T_{\alpha\beta}^+ \end{bmatrix} \begin{bmatrix} u_\alpha \\ u_\beta \end{bmatrix} = \frac{1}{2}\begin{bmatrix} 1 & -q \\ q & 1 \end{bmatrix}\begin{bmatrix} u_\alpha \\ u_\beta \end{bmatrix} = \frac{1}{2}\begin{bmatrix} D(s) & -Q(s) \\ Q(s) & D(s) \end{bmatrix}\begin{bmatrix} u_\alpha \\ u_\beta \end{bmatrix} \quad (26)$$
$$= \frac{1}{2}\frac{k_{SOGI}\omega'}{s^2 + k_{SOGI}\omega' s + \omega'^2}\begin{bmatrix} s & -\omega' \\ \omega' & s \end{bmatrix}\begin{bmatrix} u_\alpha \\ u_\beta \end{bmatrix}$$

$$\begin{bmatrix} u_\alpha^- \\ u_\beta^- \end{bmatrix} = \frac{1}{2}\frac{k_{SOGI}\omega'}{s^2 + k_{SOGI}\omega' s + \omega'^2}\begin{bmatrix} s & \omega' \\ -\omega' & s \end{bmatrix}\begin{bmatrix} u_\alpha \\ u_\beta \end{bmatrix} \quad (27)$$

As can be seen from Equations (26) and (27) positive and negative sequence components from the grid voltage vector can be calculated with help of DSOGI. However, the above Equations assume that the grid frequency corresponds to the resonance frequency ω'. The resonance frequency of the filter is adapted to the grid frequency using FLL.

C. FLL

The operation principle of FLL can be understood by investigating transfer functions $Q(s)$ and $E(s)$ in (24) and (25) respectively. The bode plots of the transfer functions $Q(s)$ and $E(s)$ are shown in Fig. 10 when ω' is 2π*50Hz.

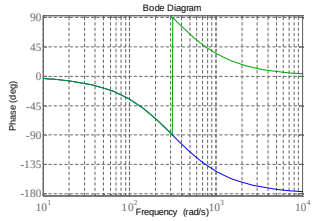

Fig. 10. Phases of $Q(s)$ and $E(s)$ when ω' is 2π*50Hz.

The phases of both transfer functions are in-phase to each other when the grid frequency is under the ω'. When the grid frequency is higher than the ω' the phases of $Q(s)$ and $E(s)$ are opposite. In other words, the transfer function values have different sign. The product of ε_{SOGI} and qv' is used as an error signal for FLL ε_{FLL}. Thus, when the grid frequency is under the ω' the ε_{FLL} has positive value and when the grid frequency is over the ω' the ε_{FLL} has negative value. The error measure ε_{FLL} is fed to the integral controller with a negative gain $-\gamma$. Thus, the positive error measure makes the controller to decrease the resonance frequency and vice versa. The error measure ε_{FLL} is zero when the filter resonance frequency corresponds to the grid frequency. The error measure ε_{FLL} used is the average of error measures of α and β axis: [3]

$$\varepsilon_{FLL} = \frac{1}{2}\left(\varepsilon_{FLL\alpha} + \varepsilon_{FLL\beta}\right) = \frac{1}{2}\left(\varepsilon_{SOGI\alpha} qu'_\alpha + \varepsilon_{SOGI\beta} qu'_\beta\right) \quad (28)$$

The structure of FLL is expressed in Fig. 11.

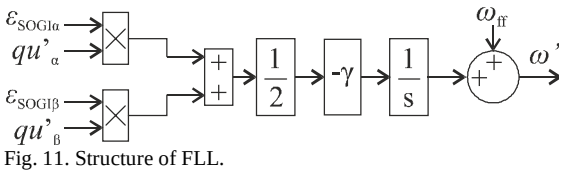

Fig. 11. Structure of FLL.

D. DSOGI-FLL

The concept of DSOGI-FLL synchronization system contains positive and negative sequence calculation using (20) and (22), two SOGIs to generate the 90 degrees shifted versions from the grid voltage and FLL to lock the resonance frequency of the SOGI to the grid frequency. The angle of the positive sequence fundamental frequency component used to synchronize the control system is calculated from the positive sequence αβ-components as follows:

$$\theta_{sync} = \tan^{-1}\left(\frac{u_\beta^+}{u_\alpha^+}\right) \quad (29)$$

The block diagram of the DSOGI-FLL is expressed in Fig. 12.

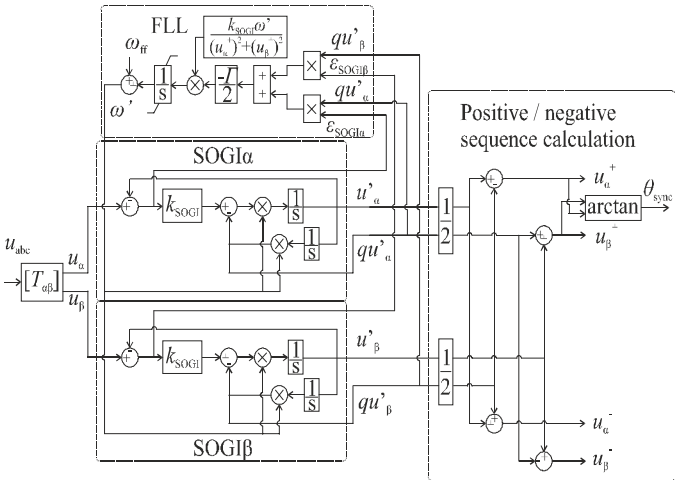

Fig. 12. Block diagram of the DSOGI-FLL.

The FLL dynamic response is affected by the square of the grid voltage, the SOGI gain and the resonance frequency of the SOGI. Thus, normalized FLL gain Γ is used which is: [3]

$$\Gamma = \frac{U^2\gamma}{k_{SOGI}\omega'}. \quad (30)$$

E. Comparison of DDSRF and DSOGI

The transfer function of positive sequence voltage vector from the grid voltage vector is calculates in (26) when the DSOGI is used. The calculation of the same transfer function when the DDSRF is used is very much space consuming and far beyond from the scope of this work. Fortunately, in the reference [3] the transfer function has been calculated and it is used in this work in order to find the relationship between DSOGI and DDSRF. The transfer function of DDSRF in αβ-coordinates can be expressed as follows:

$$\begin{bmatrix} u_\alpha^+ \\ u_\beta^+ \end{bmatrix} = \frac{\omega_f}{s^2 + 2\omega_f s + \omega'^2}\begin{bmatrix} s & -\omega' \\ \omega' & s \end{bmatrix}\begin{bmatrix} u_\alpha \\ u_\beta \end{bmatrix} \quad (31)$$

where the ω' is the frequency detected by the PLL. It can be seen from the expressions (26) and (31) that the transfer functions of DSOGI and DDSRF are same when following selection for SOGI gain is chosen:

$$k_{SOGI} = \frac{2\omega_f}{\omega'} \quad (32)$$

However, the operation of DSOGI depends on the FLL performance and the operation of DDSRF depends on the PLL performance.

V. SIMULATION MODEL

The network model used in the study is shown in Fig. 13. The feeder 1 has greater impedance compared to feeder 2 representing weak feeder. The feeder 1 impedances including transformer TF1 are chosen so that when circuit breakers Cb_{f21} and Cb_{f22} are opened the feeder impedance equals to the impedance found in real Finnish network. The feeder 2 impedances are measured from the real network. The WT system model including the control system of the NSC is shown in Fig. 14.

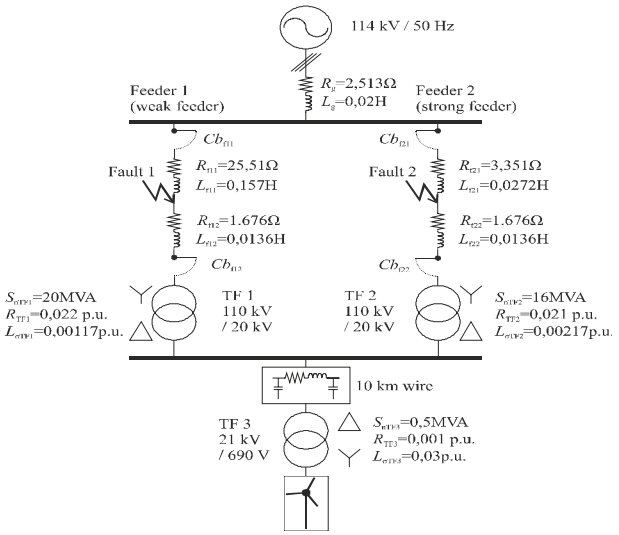

Fig. 13. Network model with used parameters.

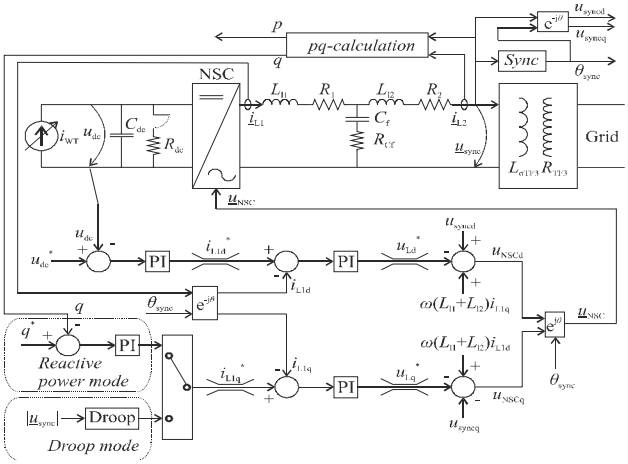

Fig. 14. Control system model of NSC.

Detailed discussion about the WT system model is carried out by the Authors in [7]. The used parameter values for the LCL-filter and NSC can also be found from [7].

VI. SIMULATION CASE

The operation of synchronizing methods during three-phase and two-phase faults occurring on the point Fault 2 in Fig. 13 are investigated. In addition, the performance of synchronizing methods under the impact of 5th network voltage harmonics is evaluated. The purpose is to find out the factors that should be taken into account when the parameters of the synchronizing methods are selected. The synchronizing frequency ω_{sync} and DSOGI resonance frequency ω' are limited to 2π*(50Hz±10Hz) rad/s. In addition, the SRF-PLL and DDSRF-PLL use PI-controller with antiwind-up which is expressed and its importance is discussed in detail by the Authors in [7]. The used antiwind-up tracking time constant was chosen to be $T_t=T_i$.

It is assumed that during voltage dip the network protection is based on distance protection with the following operation procedure. The fault occurs in point Fault 2 at 0.3s. After 200 ms from the beginning of the fault at 0.5s the circuit breaker Cb_{f22} opens and the WT currents flow through strong feeder 2. After 300ms from the fault beginning at 0.6s the Cb_{f21} opens and the fault is cleared from the WT viewpoint. [8] The control principle of NSC is chosen such that the reactive power is prioritized during the grid fault. Thus, the reference of NSC current q-component is increased to 591A and the current i_{WT} in Fig. 14 is set to zero during the fault.

The fundamental frequency negative sequence component and harmonic components from 2nd to 20th from the converter current are integrated (summed) in order to measure the quality of the generated current. In other words, the converter current is more close to pure sine wave throughout the fault when the distortion sum is small. During three and two phase grid faults the time interval for integration is from 0.3s to 0.7s while the time interval is 0.3s to 0.6s when the impact of voltage harmonics is investigated. The distortion sums are normalized using normal (Gaussian) distribution.

A. Three-phase fault

The normalized distortion sums when SRF-PLL is used are shown in Fig. 15a. As expressed in (5) the performance of the SRF-PLL depends on the selection of damping factor ζ and undamped natural frequency ω_n. Comparison is carried out using three different values for ζ i.e. 0.5, 0.707 and 1. Four different values of ω_n are located on x-axis i.e. 2π*5Hz, 2π*15Hz, 2π*30Hz, 2π*50Hz. The performance of DDSRF-PLL depends on the SRF-PLL loop parameters ζ and ω_n as well as on the low-pass filter cut-off frequency ω_f of the decoupling network shown in Fig. 7. The normalized distortion sums of DDSRF-PLL are shown in Fig. 15b and 15c when ω_f is set to $\omega_f=2\pi$*50/4 and $\omega_f=2\pi$*50/sqrt(2).

The normalized distortion sums when DSOGI-FLL is used are shown in Fig. 15d which performance depends on the parameters k_{SOGI} and Γ. The x-axis consists of Γ values which are chosen such that the bandwidth of the FLL loop is same the bandwidth of the PLL loop. For example, the bandwidth of the closed SRF-PLL loop is 64.5rad when settings are ω_n=5Hz and ζ=0.707. Hence, the bandwidths of PLL and FLL loops are comparable. However, the input of the PLL is angle and the input of the FLL is frequency. The parameter values for k_{SOGI} are chosen based on (32) in order to have same transfer functions for DSOGI and DDSRF.

The bandwidth of the SRF-PLL loop increases as the ω_n increases. Hence, the PLL tracks the grid angle earlier and the distortion sum from the measured time span decreases as can be seen from Fig. 15a. Due to the impact of zero in (9) the

effect of damping factor to the distortion sum increases as the ω_n decrease.

When DDSRF-PLL is used the distortion sums shown in Figs. 15b and 15c are significantly lower than in SRF-PLL case, especially when ω_n is small. In addition, the impact of ω_n to distortion sum is of less importance than in SRF-PLL case. When the cut-off frequency of the low-pass filter is increased from $\omega_f=2\pi*50/4$ to $\omega_f=2\pi*50/\text{sqrt}(2)$ the distortion sums generally increases due to the increased impact of network voltage phase angle jump on the synchronizing angle.

When the DSOGI-FLL is used the gain k_{SOGI} plays more essential role than the normalized gain of FLL loop Γ as can be seen from the Fig. 15d. If the k_{SOGI} is selected to be small the tracking of the grid angle takes clearly longer and distortion sums increase.

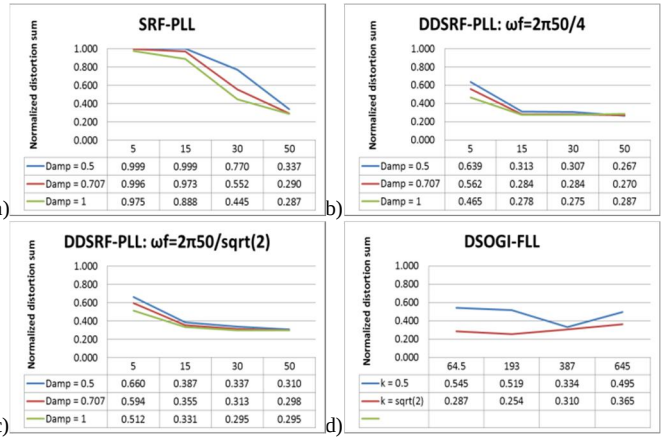

Fig. 15. Normalized distortion sums under three-phase fault: a) SRF-PLL, b) DDSRF-PLL $\omega_f=2\pi*50/4$, c) DDSRF-PLL $\omega_f=2\pi*50/\text{sqrt}(2)$, d) DSOGI-FLL.

B. *Two-phase fault*

Next, the performances of the synchronizing methods are compared during two-phase fault occurring on point Fault 2 in Fig. 13. The distortion sums when SRF-PLL is used are shown in Fig. 16a. It can be noticed that the nonlinearity of converter current increases as the ω_n and the ζ increase because the SRF-PLL is more prone to react on the negative sequence component of the grid voltage. Thus, in order to keep the amount of current harmonics small the bandwidth of the SRF-PLL should not be increased too much.

Due to the fact that the decoupling network cancels the effect of grid voltage negative sequence component when DDSRF-PLL is used the increase in ω_n and ζ do not have noteworthy impact on the distortion sums as shown in Figs. 16b and 16c. Compared to SRF-PLL the distortion sums using DDSRF-PLL are significantly lower. Thus, the performance during asymmetrical grid faults is improved. The distortion sums during the use of DSOGI-FLL are shown in Fig. 16d.

It can be noticed that the FLL gain Γ do not have great impact on the nonlinearity of the converter current. The distortion sums are lower when higher k_{SOGI} is used due to the faster tracking of the grid voltage positive sequence component angle. The results between DDSRF-PLL and DSOGI-FLL are quite similar with each other.

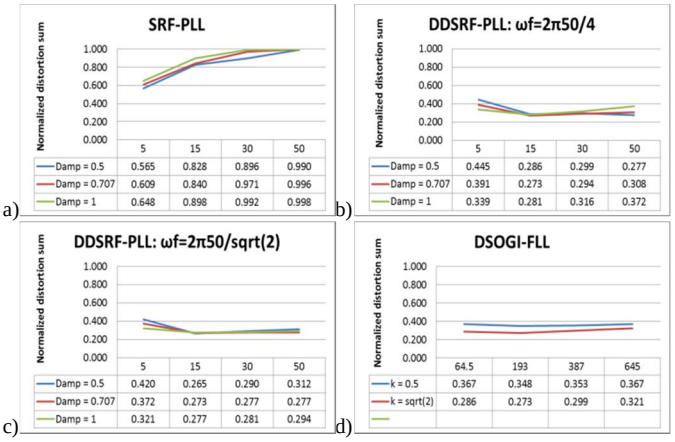

Fig. 16. Distortion sums under asymmetrical fault: a) SRF-PLL, b) DDSRF-PLL $\omega_f=2\pi*50/4$, c) DDSRF-PLL $\omega_f=2\pi*50/\text{sqrt}(2)$, d) DSOGI-FLL.

C. *Impact of 5th Grid Voltage Harmonics*

Next, the grid voltage is affected by 5th harmonics. The 5th voltage harmonics level measured from the primary side of the WT transformer was 5.91% without WT connection. The limit for 5th voltage harmonics in medium voltage network defined in standard EN 50160 is 6%. [9] Only weak feeder 1 is in operation.

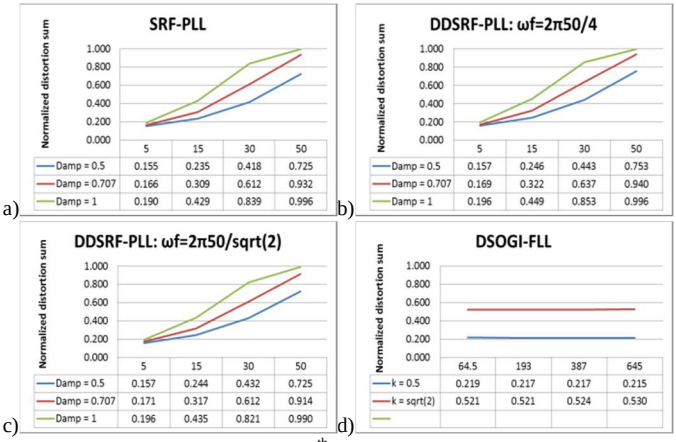

Fig. 17. Distortion sums under 5th voltage harmonics: a) SRF-PLL, b) DDSRF-PLL $\omega_f=2\pi*50/4$, c) DDSRF-PLL $\omega_f=2\pi*50/\text{sqrt}(2)$, d) DSOGI-FLL.

The distortion sums under 5th voltage harmonics when SRF-PLL is used are shown in Fig. 17a. The distortion sums under the use of DDSRF-PLL are shown in Figs. 17b and 17c. The converter current distortion increases significantly with both methods as ω_n and ζ increases. In addition, the simulation results between both methods are similar. The decoupling network used in DDSRF-PLL cancels only negative sequence component of the grid voltage fundamental component. Thus, the capability of SRF-PLL and DDSRF-PLL to generate only fundamental frequency positive sequence current depends directly on the parameters ω_n and ζ. According to simulation results of Figs. 17a-c, the presence of network voltage harmonics may be a limiting factor for the parameters ω_n and ζ when methods SRF-PLL and DDSRF-PLL are used. The simulation results when DSOGI-FLL is used are shown in Fig. 17d. The harmonic rejection capability depends on the parameter k_{SOGI} while the FLL gain Γ has no influence. Thus,

no reason for bandwidth reduction for frequency locking loop exists.

D. Selection of Parameters

As can be seen from the simulation results shown in section 6 the parameter selection for each synchronizing method is a trade-off between the performance during different faults and under the presence of network voltage harmonics. Next, the normalized distortion sums of each case are added together in order to find parameters which minimize the converter current harmonics when all cases above are taken into account. The resulting distortion sums when SRF-PLL, DDSRF-PLL (ω_f=2π*50/4), DDSRF-PLL (ω_f=2π*50/sqrt(2)) and DSOGI-FLL is used are shown in Figs. 18a, 18b, 18c and 18d, respectively.

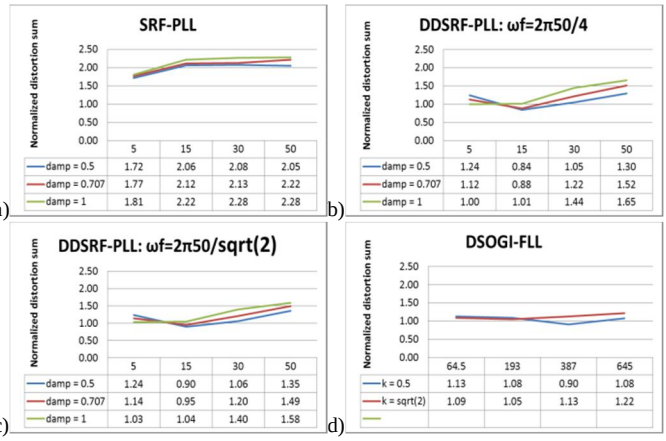

Fig. 18. Sum of distortion sums: a) SRF-PLL, b) DDSRF-PLL ω_f=2π*50/4, c) DDSRF-PLL ω_f=2π*50/sqrt(2), d) DSOGI-FLL.

As can be seen from the Fig. 18a, the distortion sums increase as the phase locking loop bandwidth increase. Although the performance of SRF-PLL with high bandwidth is better during symmetrical voltage dips the poor performance under asymmetrical voltage dips and under the presence of network voltage harmonics causes limitations for the bandwidth. In this study, the lowest overall value for distortion sum for SRF-PLL is achieved using parameters ω_n=2π*5 and ζ=0.707. In the case of DDSRF-PLL, there is no reason to limit the ω_n due to the performance during asymmetrical voltage dips. However, the performance under the presence of harmonics decreases significantly if too high bandwidth is used.

In this study, the lowest overall distortion sum values are found with parameters ω_n=2π*15, ζ=0.5, ω_f=2π*15/4 and ω_n=2π*15, ζ=0.5, ω_f=2π*15/sqrt(2). The lowest overall distortion sum value for DSOGI-FLL is achieved using parameters: k_{SOGI} = 0.5, Γ=387. If the value SOGI gain is increased to k_{SOGI}=sqrt(2) it is beneficial to reduce the normalized FLL gain to Γ=193. The lowest distortion sum from all methods is found using DDSRF-PLL with parameters ω_n=2π*15, ζ=0.5, ω_f=2π*15/4.

The simulation results above gives clear indication on how parameter selection of synchronizing methods impacts on the WT operation. However, the parameter selection should always be done based on the network parameters and general level of voltage harmonics. For example, if the network is stronger it is possible to increase the bandwidth without significant impair of the quality of the generated currents. The results of this study are from harsh cases since the faults occurs near the WT, the level of voltage harmonics is maximum allowed in medium voltage network and the network is very weak.

VII. CONCLUSION

In this paper, the performance of WT synchronizing methods SRF-PLL, DDSRF-PLL and DSOGI-FLL during three-phase and two-phase grid faults as well as under the presence of harmonics is studied. The goal of the study is to investigate how different methods can fulfil the primary task of the WT which is to generate fundamental frequency positive sequence currents to the network. The contributions of the paper contain the analysis of the impacts of tuning parameter selection on the operation of synchronizing methods and the comparison of the methods. The study is carried out using Matlab/Simulink Simpower system. The parameters of the network model are taken from the real network. The proposal of reasonable parameter selection for each method is also presented.

It is shown in the study that the bandwidth of SRF-PLL cannot be high due to the inadequate performance during unbalanced grid fault or under the presence of network voltage harmonics. When DDSRF-PLL is used the limiting factor of phase locking loop bandwidth is the harmonics level in the grid. The operation speed and harmonic content of the generated currents of WT which use DSOGI-FLL are mainly determined by the bandpass filter gain k_{SOGI}.

REFERENCES

[1] A. Luna, C. Citro, C. Gavriluta, J. Hermoso, I. Candela, P. Rodriquez, "Advanced PLL structures for grid synchronization in distributed generation", International Conference on Renewable Energies and Power Quality (ICREPQ'12), March 2012, pp. 10.

[2] S. Gao, M. Barnes, "Phase-locked loop for AC systems: Analyses and comparisons", 6th International Conference on Power Electronics and Drives, March 2012, 6p.

[3] R. Teodorescu, M. Liserre, P. Rodriquez, *Grid converters for photovoltaic and wind power systems*, John Wiley & Sons, Ltd, 2011, 398 p.

[4] H. Akagi, E. H. Watanabe, M. Aredes, Instantaneous power theory and applications to power conditioning, John Wiley & Sons, Inc, New Jersey, 2007, 379p.

[5] Franklin, G. F., Powell, J. D., Workman, M. (1998) *Digital control of dynamic systems, 3rd edition*. Addison Wesley Longman, Inc, 742 p.

[6] V. Kaura, V. Blasko, "Operation of a phase locked loop system under distorted utility conditions", IEEE Transactions on Industry Applications, Vol. 33, No. 1, 1997, pp. 58-63.

[7] A. S. Mäkinen, H. Tuusa, "Impact of strenght of fault current path on the operationof decoupled double synchronous reference frame – phase locked loop", International Conference on Renewable Energies and Power Quality, Bilbao, March 2013, 6p.

[8] P. M. Anderson, *Power system protection*. IEEE Press in association with McGraw-Hill, 1999, 1307p.

[9] H. Markiewicz, A. Klajn, "Voltage disturbances, Standard EN 50160 – Voltage characteristics in public distribution systems", July 2004, 16p. Available October 2012: http://www.leonardo-energy.org/repository/Library/PQGuide/5.Voltage%20Disturbances/5.4.2%20Standard%20EN50160.pdf.